Atomic Energy of Canada Limited

CRACKING AND BULK MOVEMENT IN IRRADIATED URANIUM OXIDE FUEL ELEMENTS

CRFD-1156

by

A.S. BAIN

Chalk River, Ontario

September, 1963

AECL-1827

CRFD-1156

CRACKING AND BULK MOVEMENT IN IRRADIATED URANIUM OXIDE FUEL ELEMENTS

by

A.S. Bain

ABSTRACT

UO_2 pellets were fabricated with simulated circumferential or diametral cracks, and with voids formed by drilling axial or radial holes. Under irradiation the cracks healed in a region extending out slightly beyond the area of discernible grain growth. Cracks in the cooler outer annulus formed early and remained during the irradiation. Similarly voids in the outer annulus were unchanged, whereas those in the grain-growth region closed. Tungsten wire markers stayed in their original positions, demonstrating that the surrounding columnar grains in the UO_2 had not formed during the solidification of a melt. Decreases in diameter of 1 mm thick Zircaloy-2 sheathing assembled with large fuel/sheath diametral clearances were due to multi-axial stresses arising from axial elongation and the lack of diametral restraint.

This paper is to be presented
at a meeting of the
American Nuclear Society at New York
in November, 1963.

AECL-1827

Chalk River, Ontario
September, 1963

CRACKING AND BULK MOVEMENT IN IRRADIATED URANIUM OXIDE FUEL ELEMENTS

INTRODUCTION

Examinations of elements after both short and long duration irradiations (1,2) have shown a complex cracking behaviour in sintered UO_2 pellets as illustrated in Figure 1. The appearance has ranged from apparently uncracked pellets to ones showing both radial and circumferential cracking.

Calculations (3) show that solid cylindrical pellets should crack when

$$\Delta T = \frac{2\sigma(1-\mu)}{E\alpha}$$

where ΔT = temperature difference between any point of reference within the body and the curved surface

σ = modulus of rupture

α = coefficient of linear thermal expansion

E = Young's modulus

μ = Poisson's ratio

Over the temperature range of interest in a UO_2 fuel element (400 to 1600°C) α, E and μ are assumed to be constant, whereas there is some evidence that σ increases with temperature. With room temperature values for the physical constants T = 75°C to 85°C; it increases with temperature as shown in Figure 2 (5). The extrapolation in Figure 2 is based on the knowledge that UO_2 is appreciably plastic at about 1500°C (6). In one laboratory test, annular UO_2 pellets 8 mm I.D. by 26.7 mm O.D. cracked when the temperature of the outer surface was ~600°C. and there was a temperature difference of 90°C between the inner and outer surfaces; in two other runs, with the outer surface at 800°C. the ΔT was 150°C when cracking occurred (5). These results show that a UO_2 fuel element will crack when operating under the thermal stresses appropriate to power-reactor conditions and that the apparently uncracked pellets observed in some tests are anomalous.

The temperature distribution across the fuel, and hence temperature-dependent phenomena such as fission-gas release and grain growth in the uranium oxide, could be affected by cracking. The effect in practice would depend on when and where the cracks occur, and the rate and mechanism with which they can heal during irradiation.

EXPERIMENT

To obtain information on the effect of cracks on the temperature distribution in the fuel, the healing of cracks, and the movement of UO_2, we decided to irradiate pellets that had been deliberately cracked or that contained tungsten wire markers.

a) To Investigate the Effect of Circumferential Cracks

Circumferential cracks were simulated by grinding out an annular pellet and inserting another smaller pellet; clearances between the components ranged from 0.02 to 0.06 mm. Simulated cracks were spaced at different radii as illustrated in Figure 3(a). The fuel-to-sheath diametral clearance was also varied to study the effect of external pressure (sheath restraint) on the extent and rate of healing. "Cracked" pellets were alternated with intact ones in the fuel elements irradiated.

b) To Investigate the Effect of Radial Cracks

Cylindrical pellets were cut on a diametral plane and the flat surfaces so formed were polished. (see Figure 3 (b)) Duplicate assemblies were irradiated under the different applied pressures obtained by varying the fuel-to-sheath diametral clearance.

c) Bulk Movement of UO_2 Under Irradiation

Under irradiation UO_2 moves either as a result of transport through the vapour phase or by plastic flow. If movement occurs it will relieve stresses and may heal or reduce cracking. Two methods of observation were investigated.

(1) A pellet (see Figure 3(c)) was cut parallel to the axis and along the pellet length. A section taken normal to the axis would show if the cut profile was altered and hence if there had been any significant bulk movement. Other cuts were made in a transverse direction; thus different mechanisms could be separated. Plastic flow due to compressive stress would tend to close a cut towards the center of the pellet whereas vapour transport would carry oxide from the hot to the cooler regions. Pellets were assembled in elements with different fuel-to-sheath diametral clearances.

(2) Some pellets were drilled with holes parallel to the axis and situated at different radial positions as illustrated in Figure 3(d). Vapour transport would tend to move the holes toward the center of the pellet and change the hole profile. Plastic flow would tend to change its cross-sectional area. Tungsten wires were placed in some holes as markers.

d) Pellet Movement Relative to Sheath

In a previous irradiation (7) of UO_2 specimens in stainless-steel sheathing the crack pattern of the oxide surface was traced on the inner surface of the sheath. Similar effects have also been observed in specimens sheathed in Zircaloy-2. Since the markings appeared to be a deposit it was inferred that UO_2 had condensed from the vapour phase during irradiation. This was investigated by irradiating at low flux pellets with radial holes as shown in Figure 3(e). The inner surfaces of the Zircaloy-2 sheaths were cleaned and lightly etched so that any markings could be more easily distinguished. To enhance mass transfer to the sheath by sublimation, fuel elements containing these pellets were sealed under a partial vacuum.

FABRICATION

The fuel elements were assembled by the AECL Fuel Development Branch at Chalk River. Details of fuel sheathing and pellet location are given in Tables 1 and 2, and the dimensions of the pellets and elements are given in Table 3.

IRRADIATION HISTORY

The elements were irradiated in three separate loadings of pressurized-water loops in the NRX reactor. The relative positions of the elements for each loading are shown in Figure 4. In Table 4 loop operating data are listed.

POWER OUTPUT OF ELEMENT

The burn-up of each element was determined from the flux indicated by the activation of a cobalt monitor which was included as a ring around the center pellet of each element. The results, given in Table 5, were calculated by R.W. Durham for an energy release of 198 MeV/fission and were based on a cobalt cross-section of 37.3 barns for thermal neutrons (2200 m/s), a spectral index of 0.054 (8), a fast-fission ratio equal to 0.021, a value of β

i.e. $\frac{\text{Total captures in U-238}}{\text{thermal + 1/v captures in U-238}}$ of 1.48, and

a ratio of surface to mean neutron flux in the fuel of 1.11. The power output per unit length was then calculated from the element specifications and based on an energy release to the coolant of 182 MeV/fission.

First Loading

Only four of the elements were examined after the first loading, the remaining four being retained for another irradiation. An estimate of the power output per unit length of the intact elements was obtained by interpolating between the values obtained from the four which were sectioned, and assuming a cosine flux distribution in the loop. An estimate of the total calorimetric output of the loop during the first loading was then calculated. Values are given in Table 5. The total calculated output of the first loading was 86 kW, compared to a measured calorimetric output which varied from 70 to 90 kW with a time-average of 75 kW. Unfortunately, the ΔT recorder across the loop did not operate properly during this loading. In other tests the power output obtained from cobalt monitor burnup data have been in good agreement with other methods such as U-235 depletion (9) and hence were preferred in the present test.

Second Loading

The power output of the two cracked pellet elements included in the second loading were calculated from the activation of their cobalt monitors.

Third Loading

The total burn-ups of three of the four specimens re-irradiated in the third loading were obtained from the cobalt monitors and from Ce-144 analyses by R.W. Durham. The estimated burn-ups during the first loading were subtracted, giving burn-ups appropriate to the re-irradiation. The power output of the fourth specimen (CED) could not be obtained directly because the uranium oxide and the cobalt monitor had been sealed in epoxy resin to obtain longitudinal sections of the fuel.

The total output of the third loading was calculated from the burn-up data, with the power for CED being estimated from the flux distribution in the loop (10). The final value agreed well with the calorimetric output measured directly in the loop (see Tables 4 and 5).

The preferred values of the time-average heat rating

for each element are included in Table 5 in terms of $K(T_s,T_o)$*

POST-IRRADIATION EXAMINATION

Each specimen was visually examined under a low-power stereomicroscope, then measured. The lengths were taken in a vee-block equipped with a micrometer depth gauge. Diameters, profiles and circumferential ridge heights were obtained as continuous traces from linear transducers (12). Summaries of the diametral and length changes for all specimens are given in Table 6 and 7 respectively. Each specimen was cut transversely at intervals along the length and the uranium oxide examined and photographed with the stereomicroscope camera. In addition, sections from the centers of elements CEE and CED were longitudinally sectioned by cutting the sheath with a milling machine and breaking apart the two halves. After photographing, the uranium oxide was removed from one half of each and the inside of the sheath inspected. Samples of any surface deposit were collected on damp cotton batting (called wipe samples), then sent for gamma spectrometric analysis.

OBSERVATIONS ON URANIUM OXIDE FUEL

	Figure Reference
1. Radial and circumferential cracks had healed in a region extending out beyond the limit of discernible grain growth. The asymmetric grain growth (Figure 6) was also noted in an adjacent whole pellet, and was attributed to flux contours in the reactor. Where healing had occurred in the region of columnar-grain growth no trace of the original crack could be found. In the region of equiaxed-grain growth healing was visible as a band of short columnar grains. If healing occurred outside the region of discernible grain growth only an intermittent band of pores marked the original interface.	5,6 7,8 9 10
2. In pellets where there was no grain growth there was no healing of cracks and the central cores could be removed without damaging the outer annulus.	11 12,13 14

* $K(T_s,T_o) = \int_{T_s}^{T_o} k\,d\theta$ where k is thermal conductivity of UO_2 at temperature θ. Subscripts s,g, and o are added to temperature limits of integration to represent the temperatures of the surface, the position of just discernible grain growth, and the centre respectively. Derivation and use of the integral is given elsewhere (11).

3. In regions where columnar grains had grown axial and radial holes were no longer visible. 15
In regions where equiaxed grains had grown 16
and in regions where no growth had occurred the holes and also transverse and longitudinal 17
slits were still visible, although holes in the equiaxed growth region were measurably smaller.

4. The tungsten wires were still in the same 18
positions in the pellets even though there had been equiaxed- and extensive columnar-grain 19
growth around some of them. The clearances around the central wires had disappeared.

5. There was no measurable difference in the amount of grain growth in pellets where there 20
was a simulated circumferential crack outside the region of grain growth compared to an intact pellet irradiated at similar power 21
rating.

6. Traces of cracks in pellets were observed on 22
the inside of the sheath after one loading. The sheath of an element which had two irradiation cycles with an intervening examination had many more traces, but examination showed that there was duplication of many patterns giving a "double image". 23

7. Wipe samples were taken from inside the sheath at points covering two radially drilled holes. Gamma-spectrometric examination of both showed almost pure fission product Cs-137 (13).

8. A light gray ring was observed on some pellet ends. Spectrometric analysis of a sample showed a higher Ba-140, La-140 content than in a sample taken from the pellet (13).

9. In the central region of the highly rated 15
specimen which was longitudinally sectioned thin columnar grains and very large equiaxed grains occurred in an apparently random manner, both types within the same pellet.

DISCUSSION

i) Pellet Cracking

All the UO_2 pellets examined had cracked. The cracking occurred in the outer surface and, in the composite pellets,

it left the core either intact or less cracked than the outer annulus. If the power rating of the fuel was low the cracks remained throughout the test. However, if the central temperature was sufficient to produce grain growth in the UO_2 the cracks healed in the area extending out from the centre to a position slightly beyond the limit of discernible grain growth. The cracks which were seen in the grain-growth region on post-irradiation examination must have occurred on reactor shutdown, and would have healed if the specimen had been re-irradiated for a few hours. Evidence for this is given in Figure 24, which is a cross section of an element that was being irradiated when the reactor tripped (14). The reactor was started again and held at power for about three hours when it tripped again, after which the specimen was withdrawn because of a suspected defect in this element.

Observations from another test (15) have shown that apparently uncracked pellets actually are cracked and break up when shaken, as illustrated in Figure 25. Similarly the observations from the present test show that the cracked annuli from the composite pellets retain their shape when the core is removed, as shown in Figure 14. The fragments are held together either by the sheath or by interlocking with each other, or both, and the pellet acts as a unit rather than individual particles. For example, cracked pellets can rotate or slide in the sheath. In another test length measurements of cracked pellets held together by the sheath showed no change from pre-irradiation values (16). The "double image" of the cracking pattern on the inside of the sheath suggests that when re-irradiated a pellet does not crack any more, even though the second irradiation is at a significantly higher power rating.

From the measurements of discernible grain growth in adjacent pellets the presence of a simulated circumferential crack did not have any significant effect on the temperature distribution across the fuel. Taking into account the estimated errors of the grain-growth measurements and uncertainties of the heat ratings the values of $K(T_s,T_g)$ are considered to be accurate to ± 2 W/cm, which is equivalent to ± 60°C. With a heat flux of about 90 W/cm^2 at the position of the circumferential crack this would indicate a heat-transfer coefficient between the two uranium oxide surfaces of 1.5 $W/cm^2°C$, or greater, which is compatible with the estimate of 0.85 $W/cm^2°C$ or greater derived by Robertson et al (17). Decreasing the restraint by increasing the fuel-to-sheath clearances or increasing the width of the simulated circumferential crack could affect the value of the heat-transfer coefficient.

ii) Movement of UO_2

The disappearance of holes in the area of columnar-grain growth shows that there can be relocation of the uranium oxide. Tungsten wire markers placed in the holes were still at their original positions, even though they were well inside

the boundary of columnar-grain growth. For comparison, a recent test at Hanford (18) demonstrated that in regions where UO_2 had melted the heavier tungsten wires had sunk to the bottom. Thus, it has been proved that the columnar grains observed in the present elements were not formed by solidification from the melt.

The relocation of the uranium oxide was due either to plastic flow, or to vapour-phase transport. The observations (1) that the axial hole in the center of the specimen exhibiting only equiaxed-grain growth was smaller yet still round, see Figure 16, and (2) that the hotter side of the holes just out of the grain-growth region were closed (Figure 19) suggest that compressive and nearly isostatic forces can produce some plastic flow; but, if the temperature is sufficient to produce columnar grain growth, movement through the vapour phase is also possible. Around the holes just outside the area of grain growth the UO_2 did not show any unusual structures, indicating that the hole had no appreciable effect on the temperature distribution.

The disappearance of the drilled holes in the central regions indicates, but does not prove, that any large voids or pores observed during post-irradiation examination of the columnar grains had developed either on reactor shutdown, or late in the irradiation. This tentative deduction is in contrast to the hypothesis of de Halas and Horn (19). They suggest that some voids are formed in their test specimens, early in the irradiation, that the effect is due to the solidification of a molten core because of increased thermal conductivity of the columnar UO_2, and that the voids remain in place throughout the test.

iii) Fission-Product Movement

The wipe samples taken from various positions inside an element revealed that different fission products can accumulate, with Cs-137 being found on the sheath covering the radially drilled holes and Ba-140, La-140 concentrated in the deposit found on the pellet ends. It should be noted, however, that ring deposits of similar appearance have been observed on pellets irradiated for three minutes in the Hydraulic Rabbit, where a large amount of fission products would not have formed. Results from wipe samples taken from the sheath of another loop test showed typical fission-product spectra in the deposits marking the ends of the pellets (19). At the centre of a pellet the spectrum had a relatively larger amount of Cs-137, and at the position of the cobalt monitor the wipe sample from the sheath showed definite traces of Co-60.

iv) Grain Growth of UO_2

There was no apparent difference in the extent of grain growth between elements sealed under partial vacuum and

those filled with argon and irradiated at similar power ratings. The same result was found when elements were irradiated for only three minutes in the Hydraulic Rabbit facility of the NRX reactor (20). It was considered that when the fuel and sheath were touching the majority of the heat was transferred through mating asperities and not through the filling gas. However, short-term tests in the Hydraulic Rabbit (2) have shown that in paired elements there was a difference in $K(T_s,T_m)$ of about 2 W/cm with helium instead of argon as filling gas, indicating that the atmosphere in the diametral gap can have an effect on the surface temperature. In the present test it would appear that there was sufficient residual gas in the elements while they were being irradiated to have an appreciable effect on the heat transfer.

Values of $K(T_s,T_g)$ were calculated then normalized to a common fuel-surface temperature of 400°C assuming a fuel-to-sheath heat-transfer coefficient of 1.25 W/cm^2°C (21), a thermal conductivity for Zircaloy of 0.155 W/cm°C, and a coolant film drop of 20°C. In the present test all specimens with an original diametral clearance of 0.2 mm or less had a value of $K(400°C,T_g)$ = 35 ± 1 W/cm, whereas for the two specimens with a diametral clearance of ~0.3 mm the value was 4 W/cm lower, (see Table 9). It is possible that, because there was less pressure on the UO_2, the temperature for grain growth would be up to 100°C higher than for the other specimens where the fuel and sheath were in firm contact (17). This increase in T_g would be equivalent to 3 W/cm; therefore the total difference in $K(400°C,T_g)$ could have been between 4 and 7 W/cm. The 4-W/cm decrease actually observed would be due to a lower heat-transfer coefficient, and a corresponding increase of the surface temperature of the UO_2 by 120°C. Thus, in these two specimens the total temperature drop across the fuel-to-sheath interface could have been as much as 200°C, which is equivalent to a heat-transfer coefficient of ~0.5 W/cm^2°C. Another test (22) gave a similar difference in $K(T_s,T_g)$ between specimens of high and low diametral clearance.

The longitudinally split element (Figure 15) clearly demonstrates the variations in grain structure which can occur in an element irradiated with a central temperature calculated to be about 2300°C. The variations appear to be random, but closer scrutiny shows that they can be correlated with what were considered minor differences in density of the pellets, as indicated by the data at the bottom of the figure. Apparently at 98.4% of theoretical density, i.e. 1.6% porosity, large single grains form, but at 2.9% porosity the grains formed are columnar. Observations on transverse sections of fuel elements have been discussed by MacEwan (23), who proposed that the large central grains resulted from the outward migration of the boundaries of the original equiaxed grains located at the centre of the element. The columnar grains in the lower-density UO_2 could have formed because of the presence of more nucleating sites for lenticular-void migration (24). But since no lenticular voids were seen

in any cross section, the columnar grains were probably caused by some other mechanism, perhaps discontinuous growth being initiated at a temperature approximating the central temperature, as discussed by MacEwan (23).

v) Diameter and Length Changes

The length and diameter data are plotted on Figure 26. After the first loading the sheathing, which should be free-standing under the conditions of the irradiation, had shrunk in diameter. Unirradiated archive pieces of the sheathing which were heated to the loop operating temperature and then cooled showed no dimensional changes, indicating that the decrease was not due to relief of residual stresses remaining from the fabrication. The diametral decreases occurred in specimens which had an original clearance between the fuel and sheath of 0.18 mm or more, and were associated with length increases, with the larger diametral clearances resulting in greater length increases. Specimens which had an original diametral clearance of 0.5 mm had an increase in diameter and either no change or a decrease in length. When re-irradiated at higher heat ratings the diameters and lengths of all specimens increased. It would thus appear that the decrease in diameter of the 1-mm sheathing during the first loading was due to multi-axial stresses arising from the axial elongation and the lack of diametral restraint.

vi) Circumferential Ridging

After the initial loading, the heights of the circumferential ridges varied directly with the heat ratings, as shown in Figure 27, and did not appear to be influenced by either the sheath thickness or the original diametral clearance. Four of the elements were re-irradiated at higher heat ratings, and all had expanded in diameter compared to the previous irradiation. The ridge heights had also increased and were in relation to the final heat ratings, irrespective of the heights after the first loading. Again there was no noticeable variation in height due to sheath thickness or original diametral clearance.

The ridge heights recorded for specimens CEY and CEZ-2 are lower than the general curve; no definite explanation can be given for the different behaviour, but it may be due to a different history of the irradiation conditions, or the sheathing, for the second loading.

Longitudinal sections were made through two circumferential ridges. Although the uranium oxide was cracked, the pellets appeared to follow the curvature of the sheath and were no longer right cylinders but had expanded at the ends to form a slight hour-glass shape. This suggests that circumferential ridges form in accord with the pellet profile and the stresses involved are larger than the restraint imposed by 1-mm Zircaloy

plus the coolant pressure. However, from these observations it cannot be stated whether the change in shape of the pellets was the cause of the ridging or was the consequence of ridges formed by some other mechanism. It can be stated though, that the presence of cracked pellets after the first loading did not affect the positions or heights of the ridges after the elements were re-irradiated. A fuller investigation of circumferential ridging is being carried out by Veeder (25). The results of his tests should more closely define the mechanism for ridge formation.

CONCLUSIONS

1. Cracks in UO_2 healed in a region extending out slightly beyond the limit of discernible grain growth. Cracks observed in the central regions of highly rated fuel elements occurred, therefore, when the element cooled.

2. In the cooler outer annulus of UO_2 the cracks formed during the first cycle and remained essentially unchanged during the remainder of the irradiation.

3. The presence of a simulated circumferential crack had no appreciable effect on the extent of grain growth. The heat-transfer coefficient between the two UO_2 surfaces must have been equal to or greater than 1.5 $W/cm^2 °C$.

4. In the region where grain growth occurs holes or voids closed with the rate of closure being much greater at higher temperatures.

5. It has been proved that narrow columnar grains observed in the UO_2 after irradiation did not form by solidification from the melt.

6. Marked differences in the structure of the grain-growth region, after irradiation at a maximum temperature calculated to be ~2300°C, have been attributed to small variations in the density of the UO_2.

7. An increase in diametral clearance from 0.2 mm to 0.3 mm resulted in a decrease in $\int k d\theta$ of 4 W/cm, which was attributed to poorer heat transfer between the fuel and sheath, resulting in a higher surface temperature for the fuel. An additional 3 W/cm could be attributed to a higher value for T_g, because of the lack of pressure on the UO_2.

8. Fission product Cs-137 accumulated on the sheath, and high concentrations of Ba-140, La-140 were found on the ends of pellets.

9. Decreases in diameter of 1-mm sheathing were due to multi-axial stresses arising from axial elongation and the lack of diametral restraint.

ACKNOWLEDGMENT

Acknowledgment is gratefully extended to M.J.F. Notley, J.R. MacEwan and J.A.L. Robertson for many helpful discussions during the progress of the experiment; to R.W. Durham for the burn-up data; to R.C. Hawkings for the gamma spectrometric results; and to G.W. Parry for the photomicrographs of the irradiated fuel.

REFERENCES

1. Robertson, J.A.L., Bain, A.S., Stevens, W.H. and Allison, G.M., "Irradiation Behaviour of UO_2 Fuel Elements", Nuclear Metallurgy Vol. VI, AIME, November, 1959.

2. Bain, A.S., Robertson, J.A.L. and Ridal, A., "UO_2 Irradiations of Short Duration - Part II", AECL-1192, February 1961.

3. Kingery, W.J., J. Am. Ceram. Soc. 38, p. 3. 1955.

4. Belle, J., Proc. 2nd UN Intl. Conf. Peaceful Uses Atomic Energy 6, p. 569. 1958.

5. Ellington, J.P., "Temperatures, Thermal Stresses and Displacements in Solid Uranium Dioxide Rods", Brit. J. Appl. Phys. 11 p. 33, 1960 and Stoll, W., "Thermal Expansion and Cracking of UO_2 Sinters". Unpublished report. AECL-FD-60. April, 1961.

6. Armstrong, W.M., Irvine, W.R. and Martinson, R.H., "Creep Deformation of Stoichiometric Uranium Dioxide", J. Nuclear Materials 7, p. 133. 1962.

7. MacDonald, R.D. and Bain, A.S., "The Irradiation of Sintered UO_2 in 0.1 mm Stainless Steel Sheaths", AECL-1159, December 1960.

8. Westcott, C.H., "Effective Cross Section Values for Well Moderated Thermal Reactor Spectra", AECL-1101, November 1960.

9. Hart, R.G., Lounsbury, M., Jones, R.W., and Notley, M.J.F., "Comparison of Methods of Determining Burn-up in Uranium Dioxide Fuel Test Specimens", submitted to Nucl. Sci. Engg. 1963.

10. Webster, H.J., Private Communication to A.S. Bain. April 1963.

11. Robertson, J.A.L., "$\int k d\theta$ in Fuel Irradiations", AECL-807, April, 1959.

12. Christie, J. and Bain A.S., "Dimensional Measurements in Irradiated Fuel Bundles Using Differential Transformer Instrumentation" AECL-1603, August 1962.

13. Hawkings, R.C., Private communications to A.S. Bain, May 1962.

14. A detailed account will eventually be given in a report in the Exp-NRX-71400 series.

15. Data will eventually be reported in the Exp-NRX-20300 series.

16. Bain A.S., Payne, W.E. and Howieson, J., "Irradiation of UO_2 and U-2 wt % Zr Alloy in the CR-V Loop in NRX Reactor. Test CR-V-b", NEI-84, February, 1958.

17. Robertson, J.A.L., Ross, A.M., Notley, M.J.F. and MacEwan, J.R., "Temperature Distribution in UO_2 Fuel Elements", J. Nuclear Materials 7, 225, 1962.

18. Christensen, J.A. and Horn, G.R., Private communication to A.S. Bain. May, 1963.

19. deHalas, D.R. and Horn, G.R., "Evolution of Uranium Dioxide Structure During Irradiation of Fuel Rods", J. Nuclear Materials 8, 1963.

20. Notley, M.J.F. and Bain, A.S., Chalk River results to be published.

21. Ross, A.M. and Stoute, R.L., "Heat Transfer Coefficient Between UO_2 and Zircaloy-2", AECL-1552, June 1962.

22. Notley, M.J.F., "The Relative Axial Expansions Under Irradiation of Stacks of UO_2 Pellets in Zircaloy Sheaths", AECL-1598, August. 1962.

23. MacEwan. J.R., "Grain Growth in Nuclear Ceramics", Presented to the Electrochemical Society, Pittsburgh, Penn., April 1963, Text to appear as an AECL report.

24. MacEwan, J.R. and Lawson, V.B., "Grain Growth in Sintered Uranium Dioxide", J. Amer. Ceram. Soc. 45, 42, 1962.

25. Veeder, J., Chalk River work to be published in Exp-NRX-22100 series.

TABLE 1

Details of Elements

Fuel

Batch,	P 135 A-1 sintered 2.5 hours at 1650°C in cracked ammonia
O:U ratio	2.004 ± 0.003
Enrichment	1.877 ± 0.006 wt % U-235 in total U
Density	10.70 ± 0.05 g/cm^3
Average grain size	14 μm
Pellet length	19 mm (nominal)

Sheathing

Zircaloy-2	Batch SZF Nominal O.D. 20 mm wall thickness 1 mm
Zircaloy-4	Batch WZ4A Nominal O.D. 20 mm wall thickness 0.38 mm

TABLE 2

Location of Special Pellets in Elements

Element	CEB	CDX	CEA	CED	CEE	CEZ	CDZ	CEC	CEY	CEZ-2
Pellet position										
Top	f	f	f	f	f	f	f	f	f	f
2	e	f	d-1	e	e	d-1	f	e	a-2	a-2
3	f	a-1	f	f	f	f	a-1	f	f	f
4	e	f	d-2	e	e	d-2	f	e	a-1	a-1
5	f	a-2	f	f	f	f	a-2	f	f	f
6	f	f	c	f	f	c	f	f	f	f
7	e	a-3	f	e	e	f	a-3	e	a-2	a-2
8	f	f	b	f	f	b	f	f	f	f
9		a-1	f			f	a-1			
10		f	d-1			d-1	f			
11		a-2	f			f	a-2			
12		f	c			c	f			
13		d-2	f			f	d-2			
14		f	b			b	f			
15		a-3	f			f	a-3			
Bottom		f	f			f	f			

(a) Pellet containing a circumferential crack . a-1 to 2-3 indicate different crack positions as shown in Figure 3.

(b) Pellet cut longitudinally into two halves.

(c) Pellet with a longitudinal and radial slit.

(d-1) Pellet with holes drilled longitudinally parallel to the axis.

(d-2) Pellet as in d-1 but with tungsten wires in holes.

(e) Pellet having radial holes.

(f) Plain pellet

TABLE 3

Dimensions of Elements

Specimen	UO_2				Sheath			Clearances		Overall length
	length (mm)	diameter (mm)	dishing[1] (mm/mm)	weight (g)	Outer diameter minimum (mm)	Outer diameter maximum (mm)	thickness (nominal) (mm)	diametral (mm)	axial (mm)	(mm)
CEB	151.76	17.98	0.035	405.4	20.17	20.19	1.0	0.28	0.05	179.70
CDX	303.23	18.21	0.035	824.4	20.19	20.22	1.0	0.05	<0.05	336.30
CEA	305.24	18.06	0.035	814.8	20.19	20.22	1.0	0.20	0.05	337.59
CED	152.02	19.05	0.035	455.8	19.99	20.04	0.4	<0.05	0.05	179.83
CEE	151.99	18.91	0.035	449.3	19.86	20.09	0.4	0.18	0.05	179.74
CEZ	303.76	18.21	0.035	827.4	20.19	20.22	1.0	0.05	0.05	336.47
CDZ	303.48	18.06	0.035	815.7	20.17	20.22	1.0	0.20	0.05	335.86
CEC	151.66	18.06	0.035	409.5	20.17	20.19	1.0	0.20	0.05	179.69
CEY	152.02	18.06	0.022	412.6	20.18	20.22	1.0	0.20	0.05	179.64
CEZ-2	152.73	17.96	0.026	404.9	20.17	20.22	1.0	0.30	0.05	180.26

[1] The end faces of the pellets had a shallow re-entrant profile which is standard for Canadian power-reactor fuel and which provides space for axial expansion.

TABLE 4

Irradiation History

Loading	Date In	Date Out	E.F.P.D.[a]	Operating time (h)	"f"[b] factor	Moderator level (cm)	Reactor Power (MW)	Calorimetric[c] loop output (kW)
1	Oct. 24/61	Nov. 21/61	21.2	521	0.0075	290	42	70 to 90
2	July 20/62	Aug. 19/62	24.0	653.6	varied	290 ± 5	37.5	
	July 20/62	July 30/62		222.3	0.0075		37.5	68.5
	July 30/62	Aug. 8/62		160.8	0.0082		38	78.4
	Aug. 8/62	Aug. 19/62		270.5	0.0086		37	83.4
				653.6				
3	Dec. 18/62	Jan. 18/63	24.6	615.5	0.0096	290 ± 5	varied	
	Dec. 18/62	Dec. 24/62		90.4		285	42	61.0
	Dec. 24/62	Dec. 26/62					0	
	Dec. 26/62	Dec. 31/62		114.3		285	35	50.2
	Jan. 1/63	Jan. 2/63					0	
	Jan. 2/63	Jan. 19/63		410.8		290 ± 5	42	58.8
				615.5				

(a) Equivalent full power days based on 42 MW reactor power

(b) Fraction of power output of NRX reactor if metal x-rod installed in this position

(c) Calorimetric data increased by 3 kW to compensate for heat loss from test section, plus gamma heat in loop components and multiplied by $\frac{182}{185}$ to compensate for heat produced in loop components.

TABLE 5

Power Output of Elements

Specimen	Burnup at position of cobalt monitor		Power output per unit length at monitor	Total Power Output of Element	Power output including End Flux Peaking	Estimated power output of elements not sectioned	$K(T_s.T_o)$
	198 MeV/f (MWd/te U)	182 MeV/f (MWd/te U)	(W/cm)	(kW)	(kW)	(kW)	(W/cm)
1st loading							
CEB	341	314	340			5.3	26.2
CDX	435	400	438	13.3	13.5		37.7
CEA	535	492	532	16.2	16.5		41.0
CED	536	494	600			9.4	45.8
CEE	540	496	595	9.04	9.3		45.3
CEZ	500	460	505	15.3	15.6		38.8
CDZ	382	352	384			11.8	29.6
CEC	270	245	270			4.2	20.6
				Total	85.6		
2nd loading							
CEY	730	672	600	9.12	9.40		46.1
CEZ-2	740	680	596	9.10	9.37		45.8
3rd loading							
CED	832	765	802	12.2		12.6	61.0
CDZ	1270-382=888	815	766	23.2	23.6		59.0
CEB	1200-341=859	789	735	11.2	11.5		56.5
CEC	1075-270=805	740	700	10.6	11.0		53.8
				Total	58.7		

N.B. Figures underlined are estimated from flux distribution in loop

TABLE 6

Diameter and Circumferential Ridge Height Measurements

Element	Diameters						Circumferential Ridges					
							After 1st Loading			After 2nd Loading		
	Pre-Irrad. (mm)	After 1st loading (mm)	Change (mm)	After 2nd loading (mm)	Change from 1st (mm)	Change from Pre (mm)	Maximum (mm)	Minimum (mm)	Average (mm)	Maximum (mm)	Minimum (mm)	Average (mm)
CEB	20.18	20.13	-0.05	20.20	+0.07	+0.02	0.051	0.013	0.025	0.190	0.102	0.114
CDX	20.20	20.24	+0.04				0.064	0.025	0.033			
CEA	20.20	20.18	-0.02				0.063	0.038	0.051			
CED	20.02	20.10	+0.08	20.14	+0.04	+0.12	0.089	0.063	0.071	0.127	0.089	0.102
CEE	19.99[1]	19.94	-0.05				0.089	0.038	0.066			
CEZ	20.20	20.25	+0.05				0.076	0.063	0.066			
CDZ	20.19	20.17	-0.02	20.19	+0.02	0.00	0.063	0.025	0.033	0.127	0.051	0.114
CEC	20.18	20.14	-0.04	20.19	+0.05	+0.01	0.025	0.013	0.015	0.127	0.102	0.109
CEY	20.19	20.18	-0.01				0.076	0.025	0.043			
CEZ-2	20.19	20.19	0.00				0.063	0.025	0.041			

[1] Diameter of CEE varied from 18.89 to 20.09 mm before irradiation due to ovality; after irradiation the element was round.

TABLE 7

Length Measurements

Element	Pre-Irrad. (mm)	After 1st loading (mm)	Change (mm)	Change %	After 2nd loading (mm)	Change from 1st (mm)	Change from Pre-Irrad. Data (mm)
CEB	179.70	179.95	+0.25	0.14	180.57	0.62	0.87
CDX	336.30	336.20	-0.10	-0.03			
CEA	337.59	337.64	+0.05	0.015			
CED	179.84	179.88	+0.04	0.02	180.31	0.43	0.47
CEE	179.74	179.93	+0.19	0.1			
CEZ	336.47	336.09	-0.38	-0.1			
CDZ	335.86	336.09	+0.23	0.07	336.75	0.66	0.89
CEC	179.69	179.80	+0.11	0.06	180.31	0.51	0.62
CEY	179.64	179.96	0.32	0.19			
CEZ-2	180.26	180.70	0.44	0.24			

TABLE 8

Diametral Clearance Plus Change in Diameter

Specimen	Diametral Clearance	Expansion after 1st loading	Clearance + Expansion	Net Expansion after 2nd loading	Clearance + Expansion	Sheath Thickness
CEB	0.28	-0.05		0.02	0.30	1.0
CDX	0.05	+0.04	0.09			1.0
CEA	0.20	-0.02				1.0
CED	<0.05	+0.08	<0.13	0.12	<0.17	0.4
CEE	0.18	-0.05				0.4
CEZ	0.05	+0.05	0.10			1.0
CDZ	0.20	-0.02		0	0.20	1.0
CEC	0.20	-0.04		0.01	0.21	1.0
CEY	0.20	-0.01				1.0
CEZ-2	0.30	0				1.0

TABLE 9

Values of $\int_{400\,^{\circ}C}^{T_g} k\,d\theta$

Element	ratio $\frac{\text{dia. of grain growth}}{\text{dia. of pellet}}$ at mid point	$\int_{400\,^{\circ}C}^{T_g} k\,d\theta$ (W/cm)
First Loading		
CDX	no grain growth	>33.7
CEA	0.31	36
CEE	0.46	36
CEZ	0.31	35
Second Loading		
CEY	0.53	35
CEZ-2	0.60	31
Third Loading		
CED	0.65	34.0
CDZ	0.68	34.0
CEB	0.70	30.5
CEC	0.61	34.0

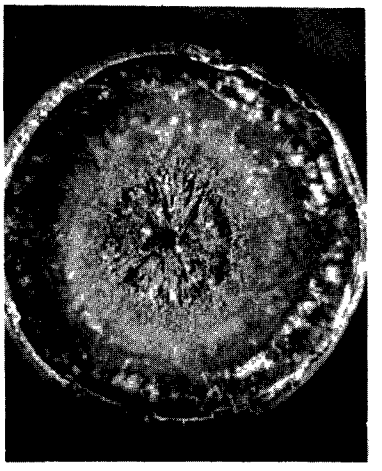

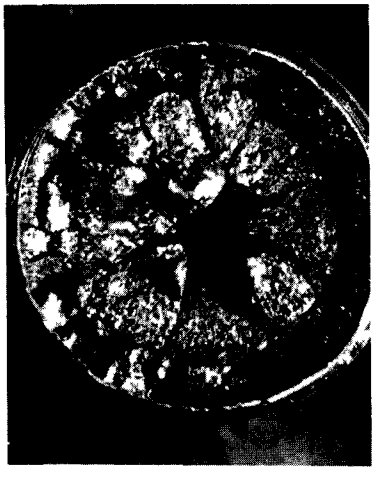

FIGURE 1: Typical Cross-sections of Irradiated Pellets

a) No apparent cracking - Low heat rating

b) No apparent cracking - central melting

c) Random cracking

d) Radial and circumferential cracking

e) Circumferential cracking.

FIGURE 2. CRITICAL TEMPERATURE FOR THERMAL CRACKING OF UO_2 (REFERENCE 5)

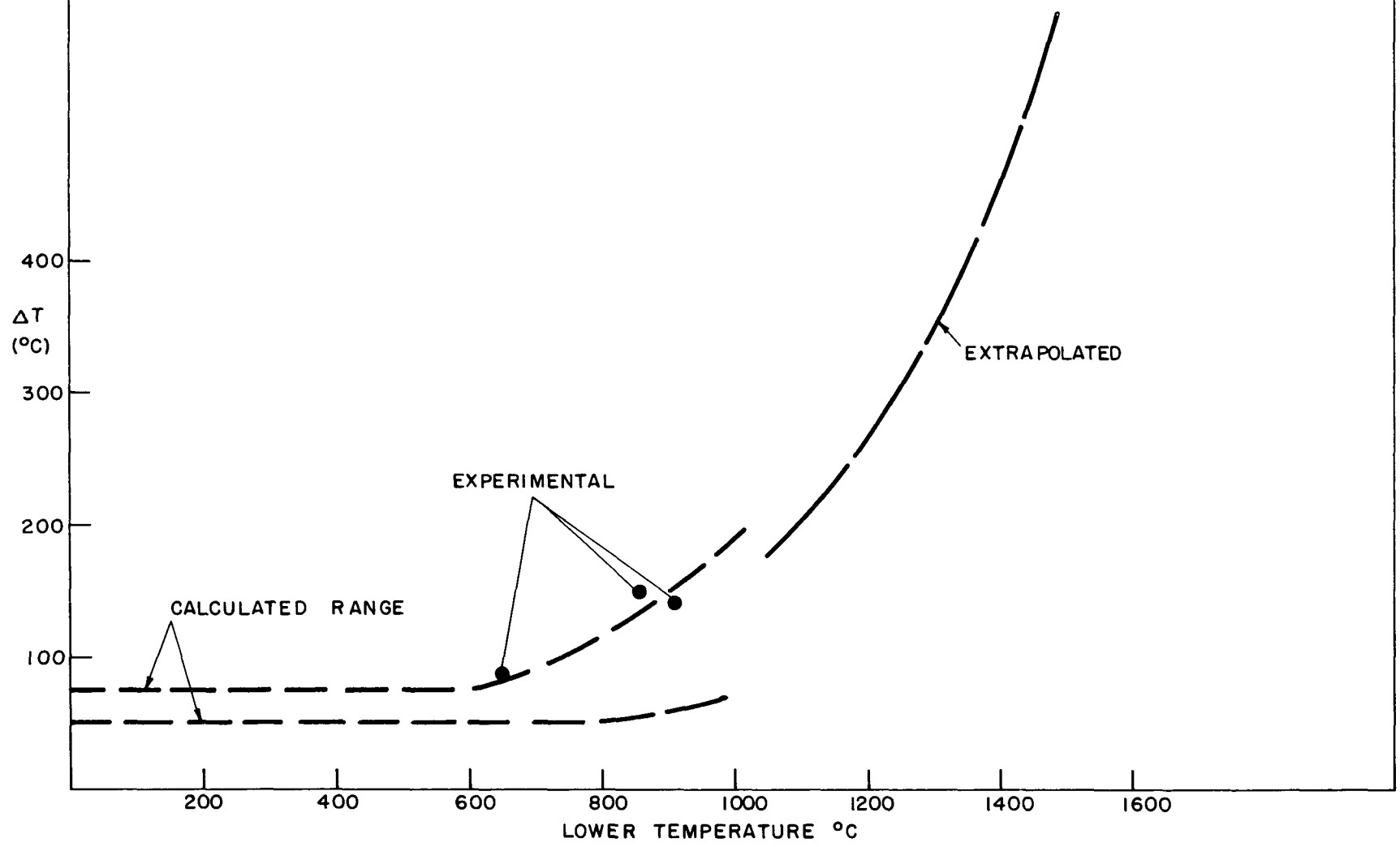

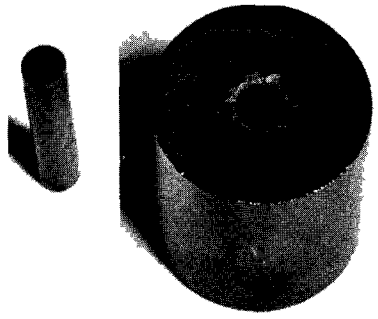

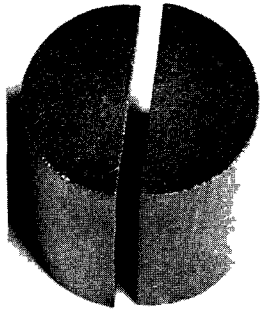

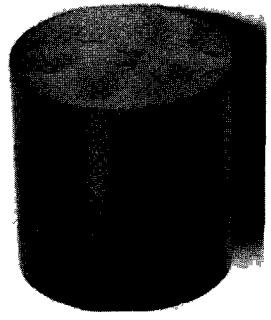

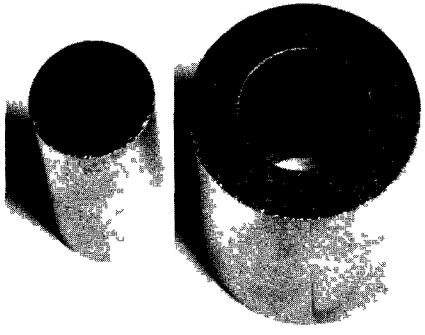

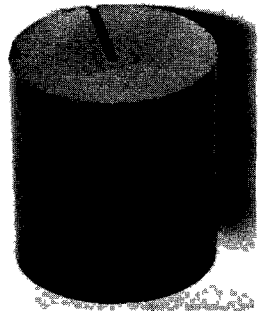

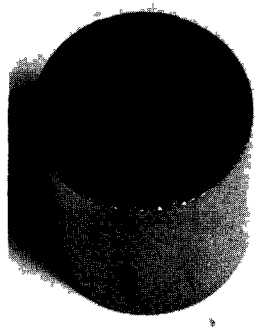

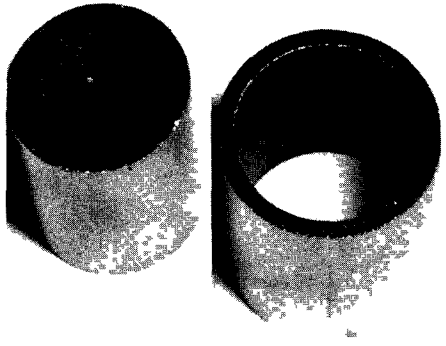

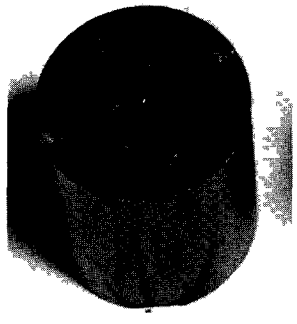

FIGURE 3: Types of Special Pellets Fabricated for Test X-20700

a-1) a-2) a-3)	Composite pellet, simulating circumferential crack.
b	Diametral crack
c	Axial and Transverse slit
d	Axial holes
e	Radial holes
f	Plain pellet

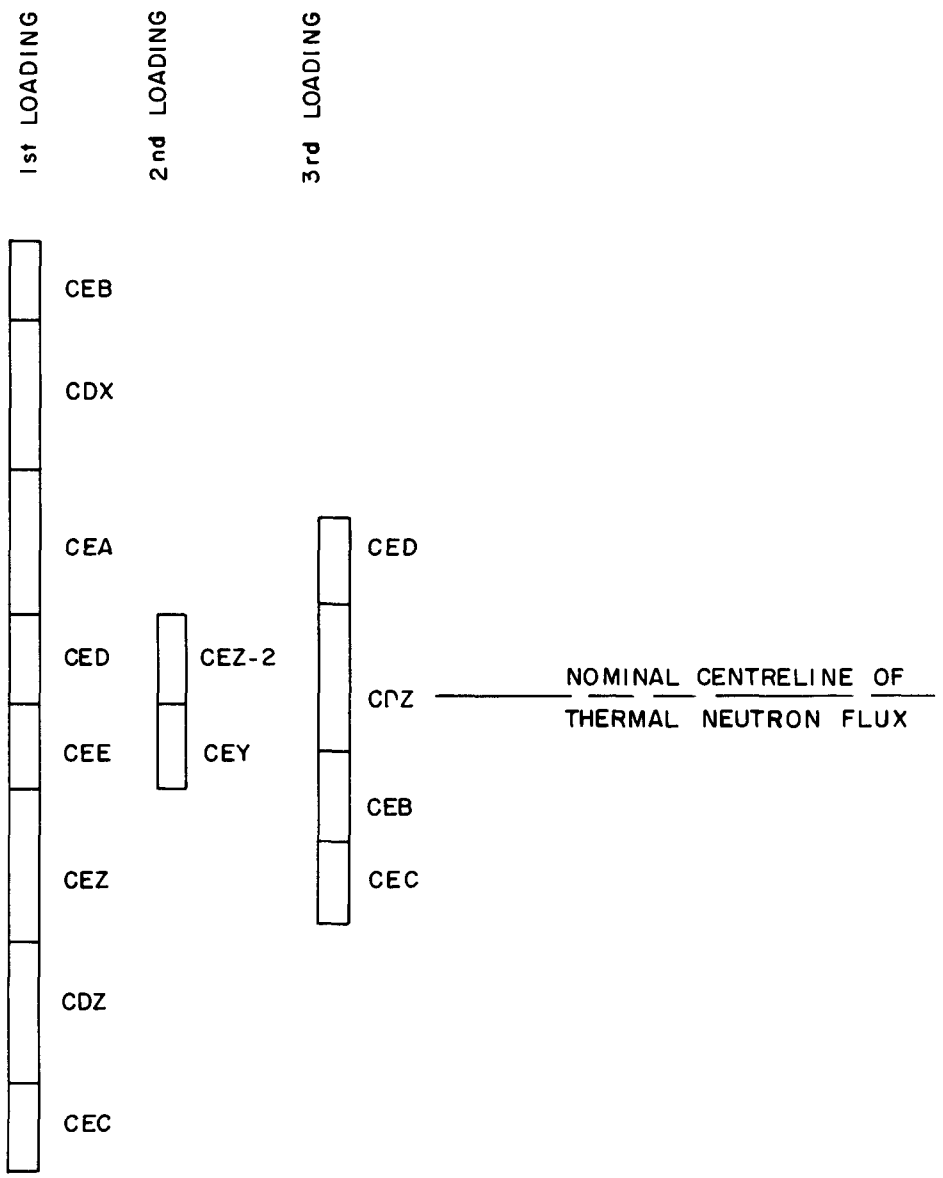

FIGURE 4. RELATIVE POSITIONS IN LOOP DURING THREE LOADINGS

FIGURE 5: Healing of diametral crack to region beyond extent of equiaxed grain growth. Element CEA.
Reference Y-66-B1 7.5X

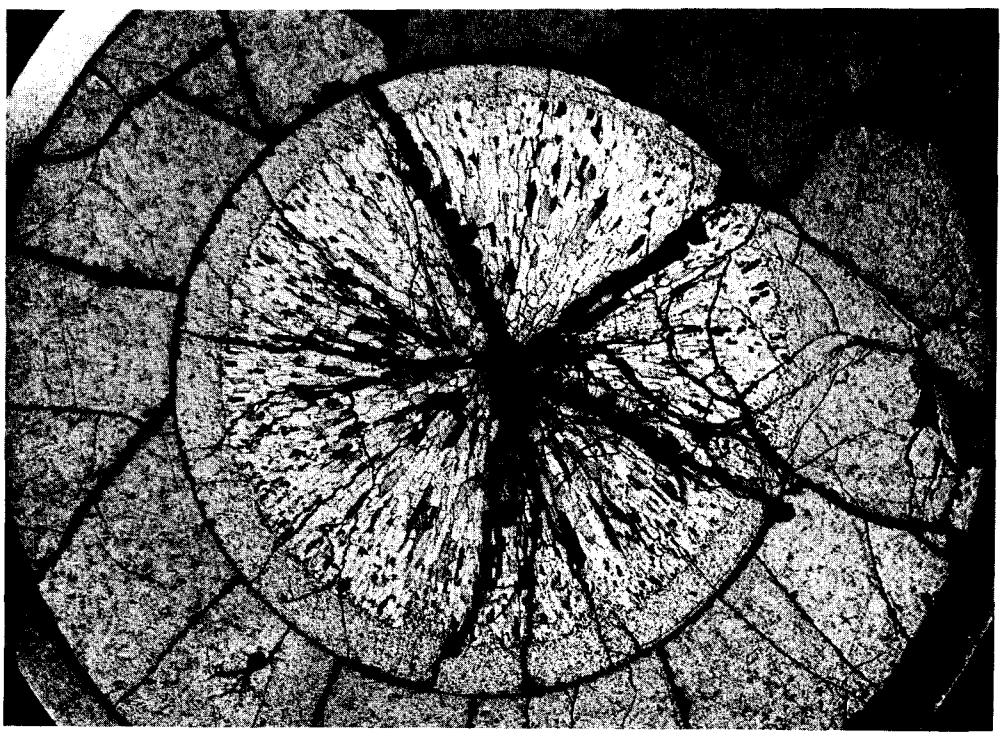

FIGURE 6: Partial Healing of Circumferential Crack Outside area of Discernible Grain Growth. Element CEZ-2.
Reference X11-E1 7.5X

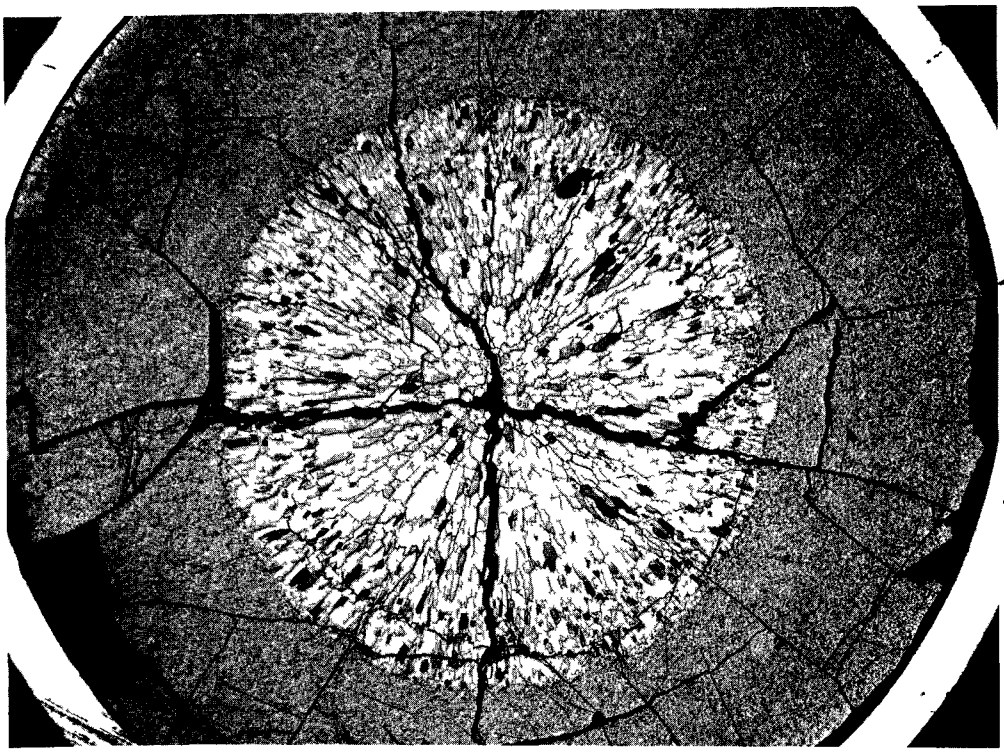

FIGURE 7: Healing of Circumferential Crack in Area of Small Columnar Grain Growth. Element CEZ-2.
Reference Y92-B1 7.5X

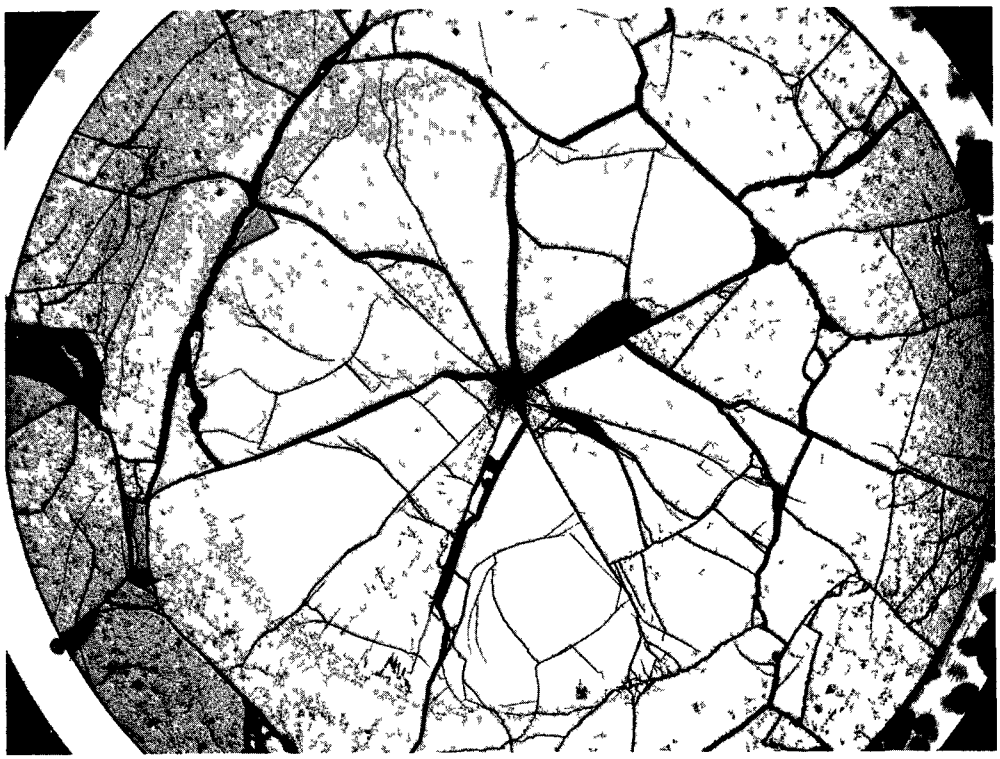

FIGURE 8: Healing of Circumferential Crack When Original Crack-diameter is Larger. Element CDZ.
Reference X-10-B1 7.5X

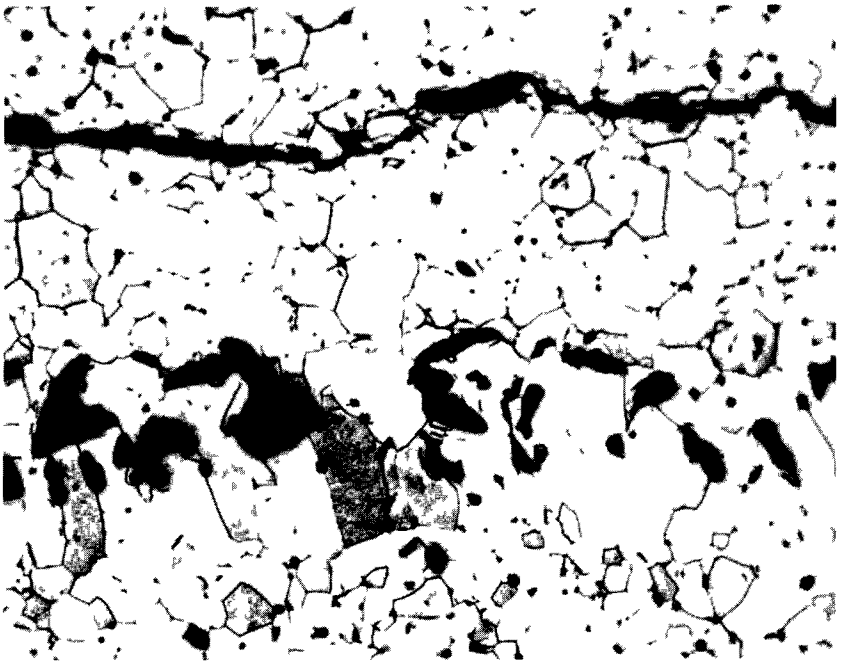

FIGURE 9: Small columnar grains formed when crack healed in equiaxed growth region. Element CEA.
Reference Y66-A1 250X

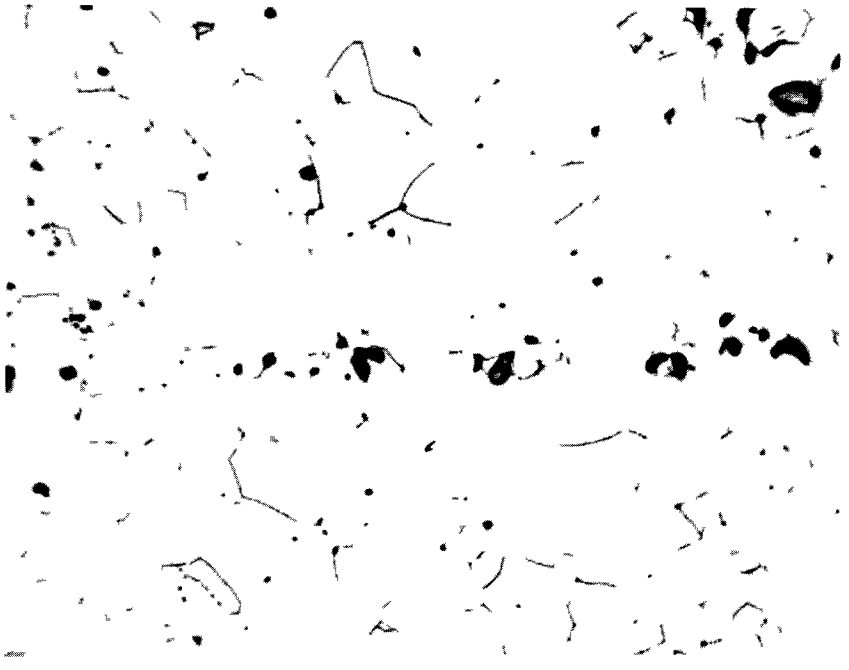

FIGURE 10: Line of pores where crack healed in area beyond any grain growth. Note change in magnification from Figure 9. Element CEZ.
Reference X11-02 500X

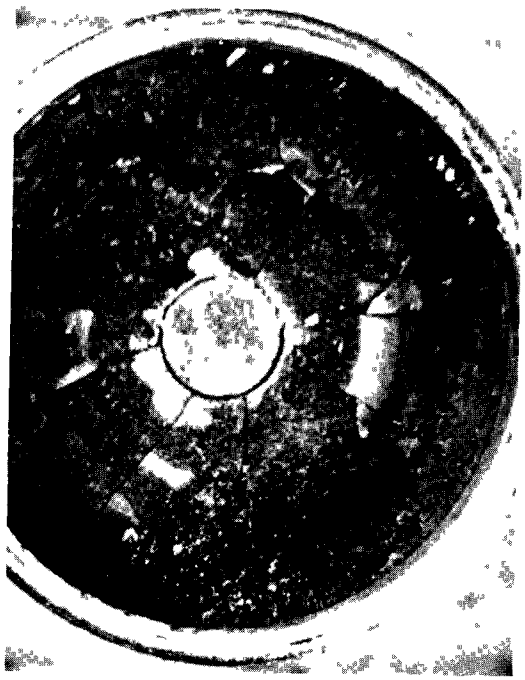

FIGURE 11: Radial cracking in Outer Annulus. No cracking in Core. Element CDX Reference 6520 4X

FIGURE 12: No healing of Diametral Crack in Pellet Irradiated at Low Rating. Element CEZ. Reference 6549 4X

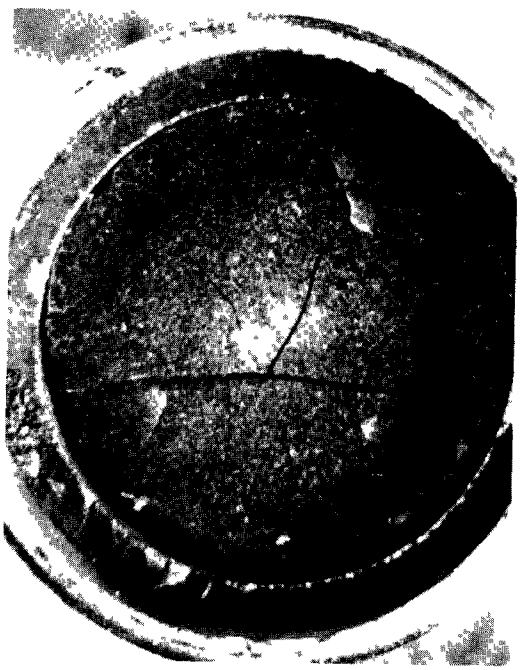

FIGURE 13: Lowly Rated Pellet in which Large Central Core was Cracked. Element CDX Reference 6515 4X

FIGURE 14: Outer Annulus of Pellet Shown in Figure 13. Element CDX Reference 6517 4X

End plug UO_2 Interface

Densities of Pellets g/cm^3	10.65	10.78	10.65	10.65	10.77	10.73	10.78	10.65
% Porosity of Pellet	2.92	1.73	2.92	2.73	1.83	2.19	1.23	2.92

FIGURE 15: Longitudinal Section of Highly Rated Element CED.

Three of the pellets had radial holes which are not visible anywhere in the central areas of the pellets, and therefore must have closed. Traces of holes were observed in the fragments of the outer annulus.

Reference 7792

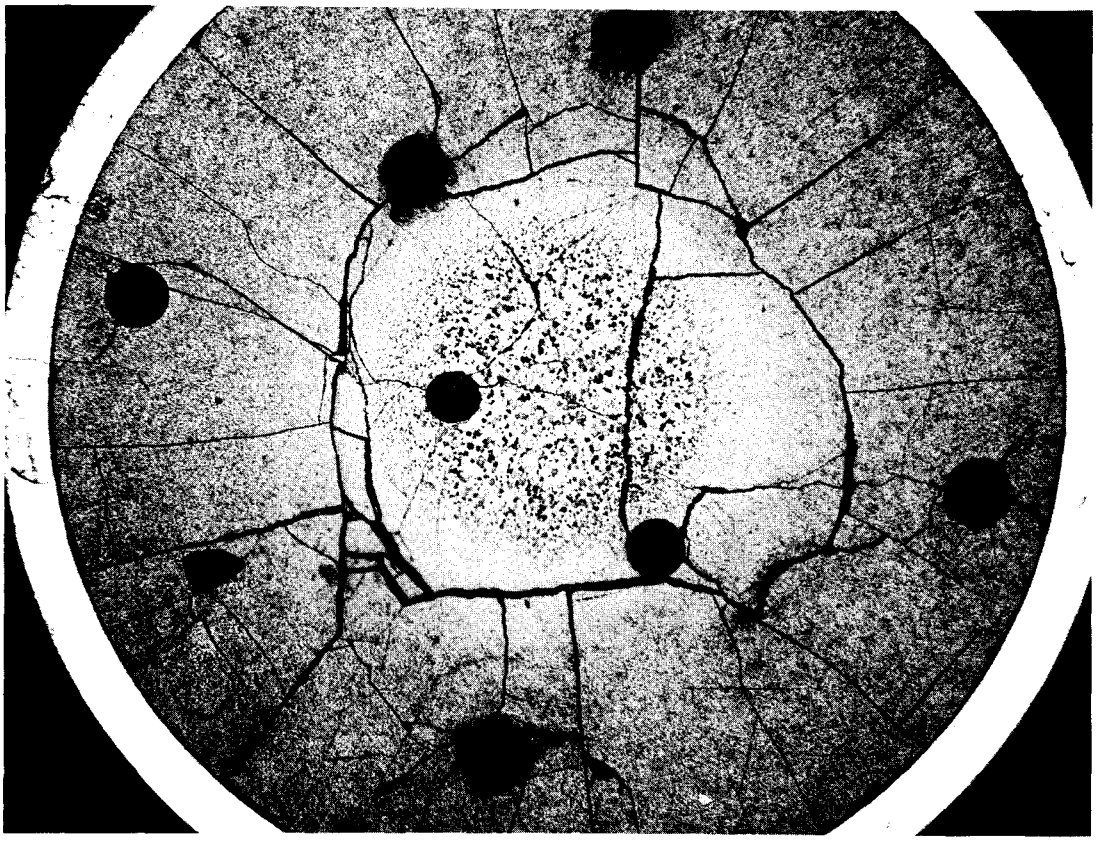

FIGURE 16: Axial holes in Pellet. Note Centre Hole is Slightly Smaller in Diameter than Others.
Reference Y39 B-2 7.5X

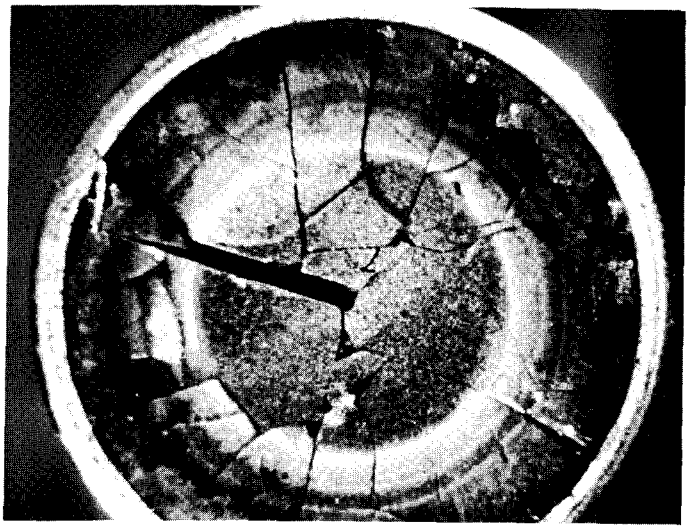

FIGURE 17: Longitudinal Slit, Showing Essentially No Change in Shape Except Rounding at Tip. Element CEZ.
Reference 6551 4X

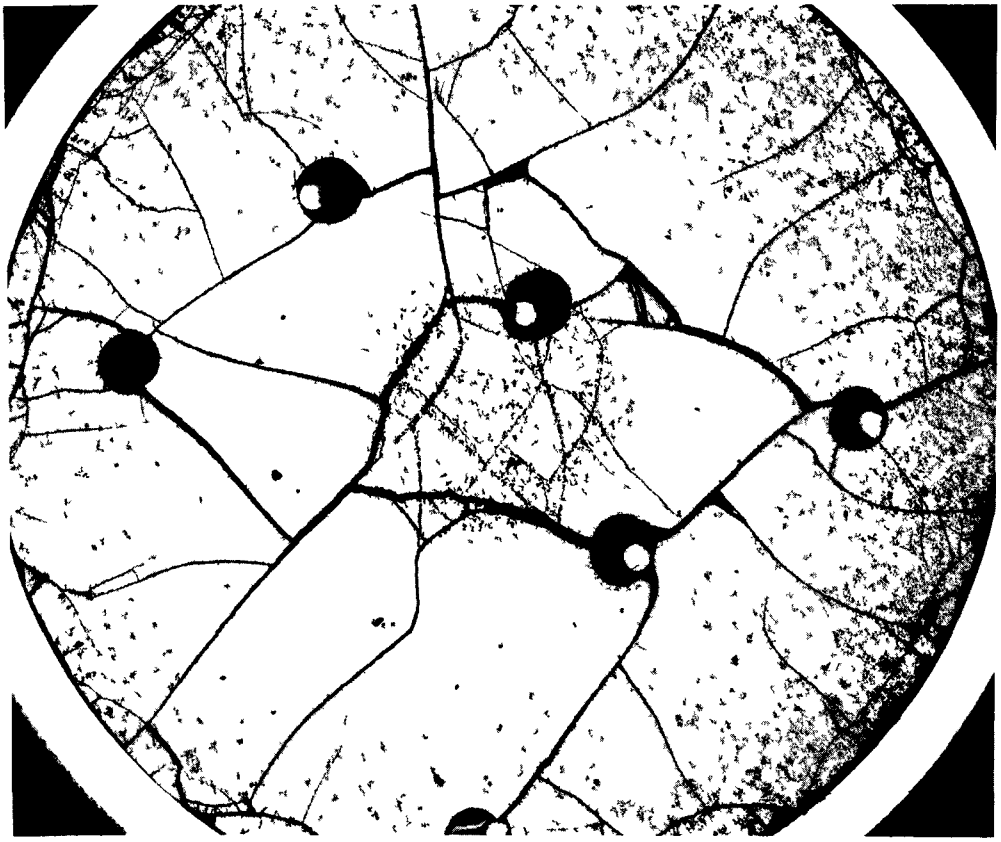

FIGURE 18: Tungsten wires in Place in Element CEA. Irradiated to Produce Equiaxed Growth. Missing Wires fell out during post-irradiation handling.
Reference X66-A2

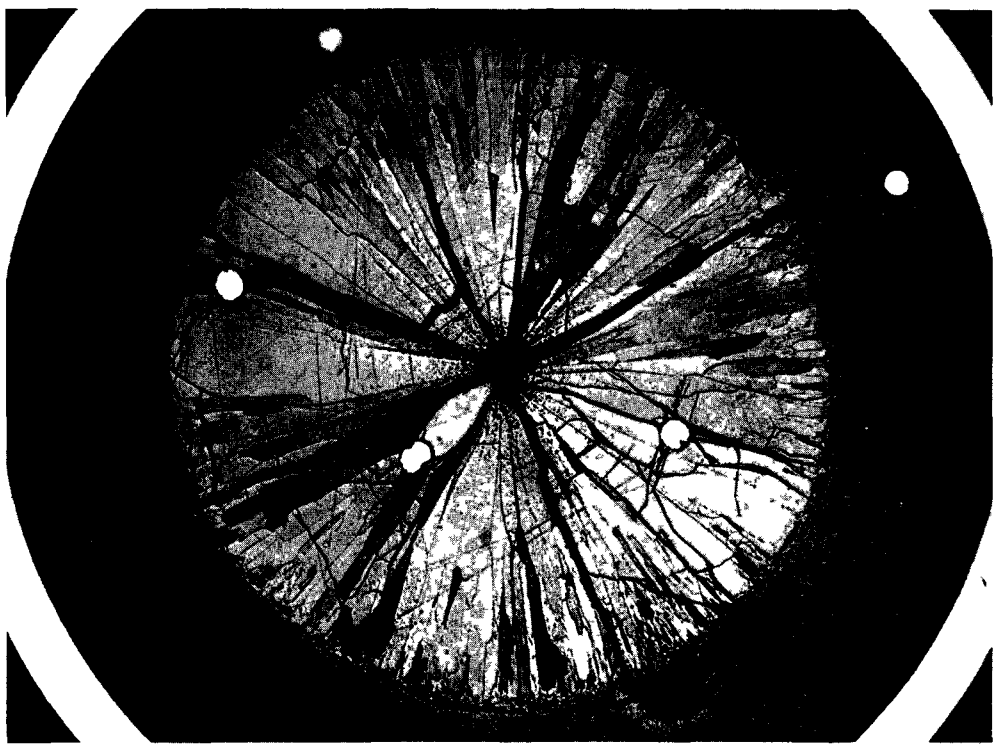

FIGURE 19: Tungsten Wires Still in Original Positions Even Though Surrounded by Extensive Columnar Grain Growth. Missing wires fell out during post-irradiation handling. Note Central Holes have Closed. Element CDZ.
Reference X10-A1 7.5X

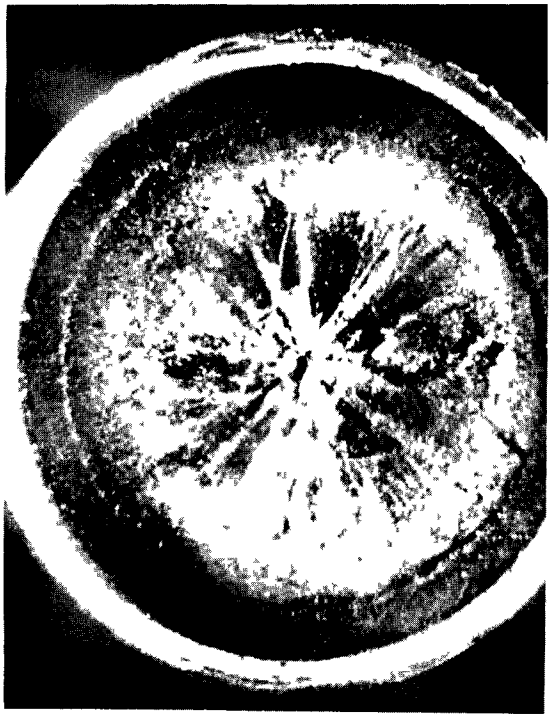

FIGURE 20: Grain Growth in Composite Pellet from Element CDZ. Note Extent of Growth is the same as that for the Pellet Shown in Figure 21.

Regerence 7751 4X

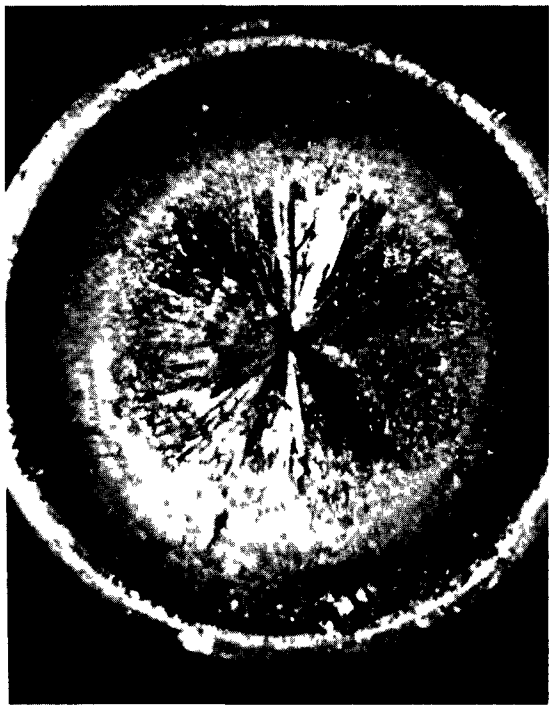

FIGURE 21: Grain Growth in Plain Pellet of Element CDZ

Reference 7743 4X

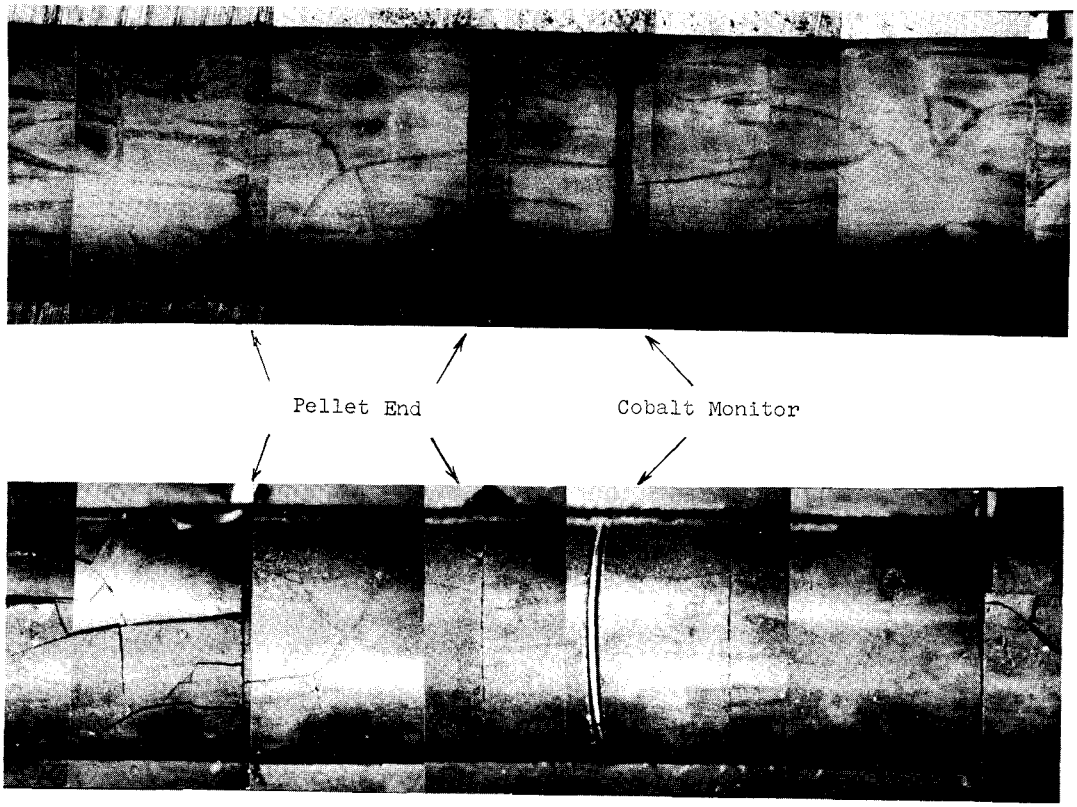

FIGURE 22: Cracked pellets and traces on sheath after one cycle of irradiation. Element GEE

Reference 6567

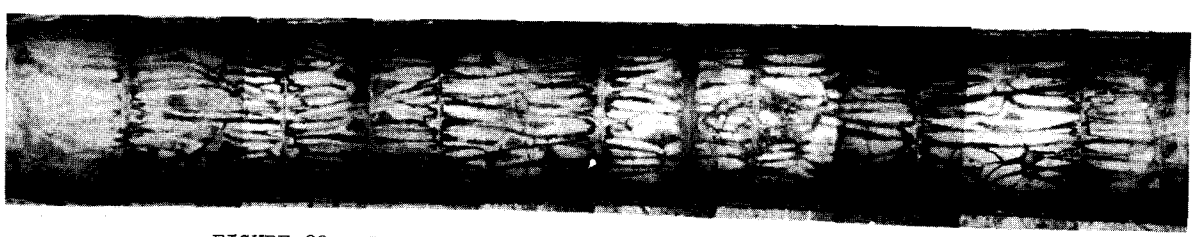

FIGURE 23: Traces on sheath after two cycles of irradiation with intervening inspection. Note "Double-Image" of pattern. Element CED

Reference 7804

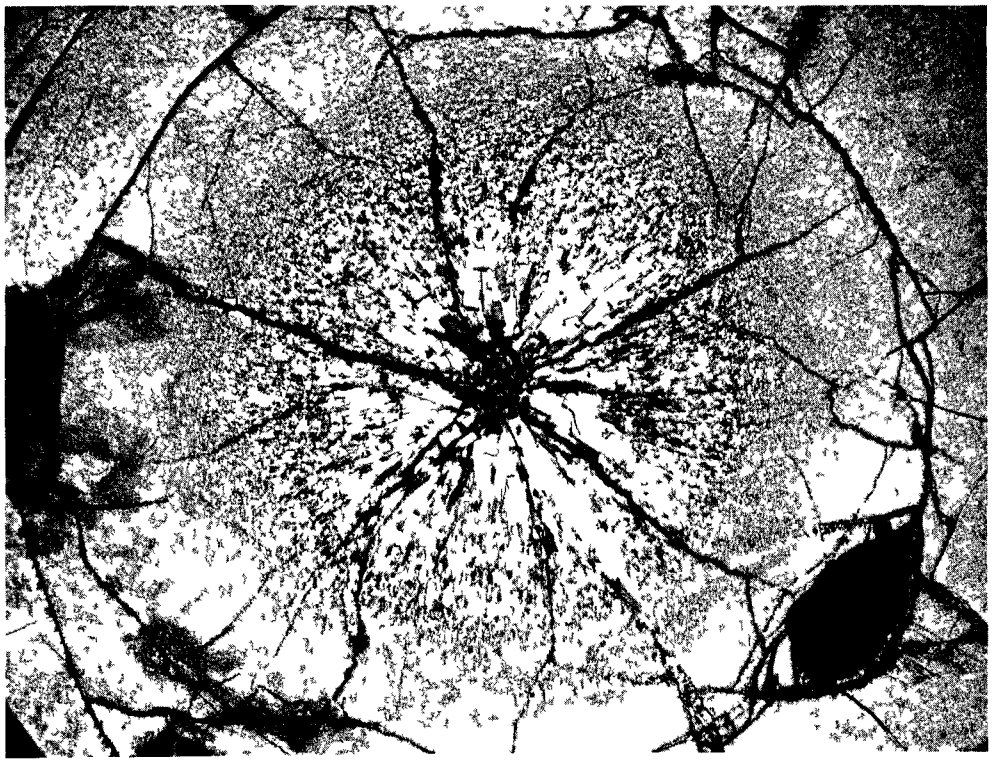

FIGURE 24: Healing of Central Cracks in Pellet which was cooled then Re-irradiated for Three Hours
Reference X14-08 12.5X

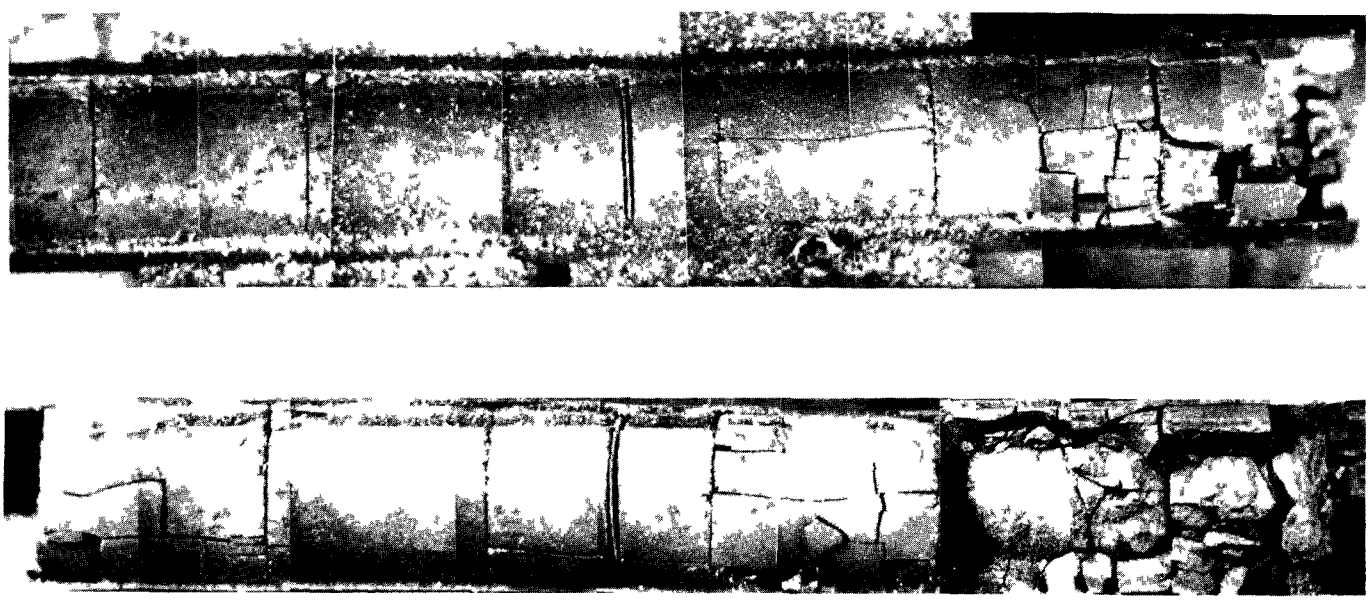

FIGURE 25: Fragmentation of Lightly Cracked or Apparently Uncracked Pellets. Top photo is after removal of sheath; bottom is after slight movement of the fuel.
Reference T2420-4

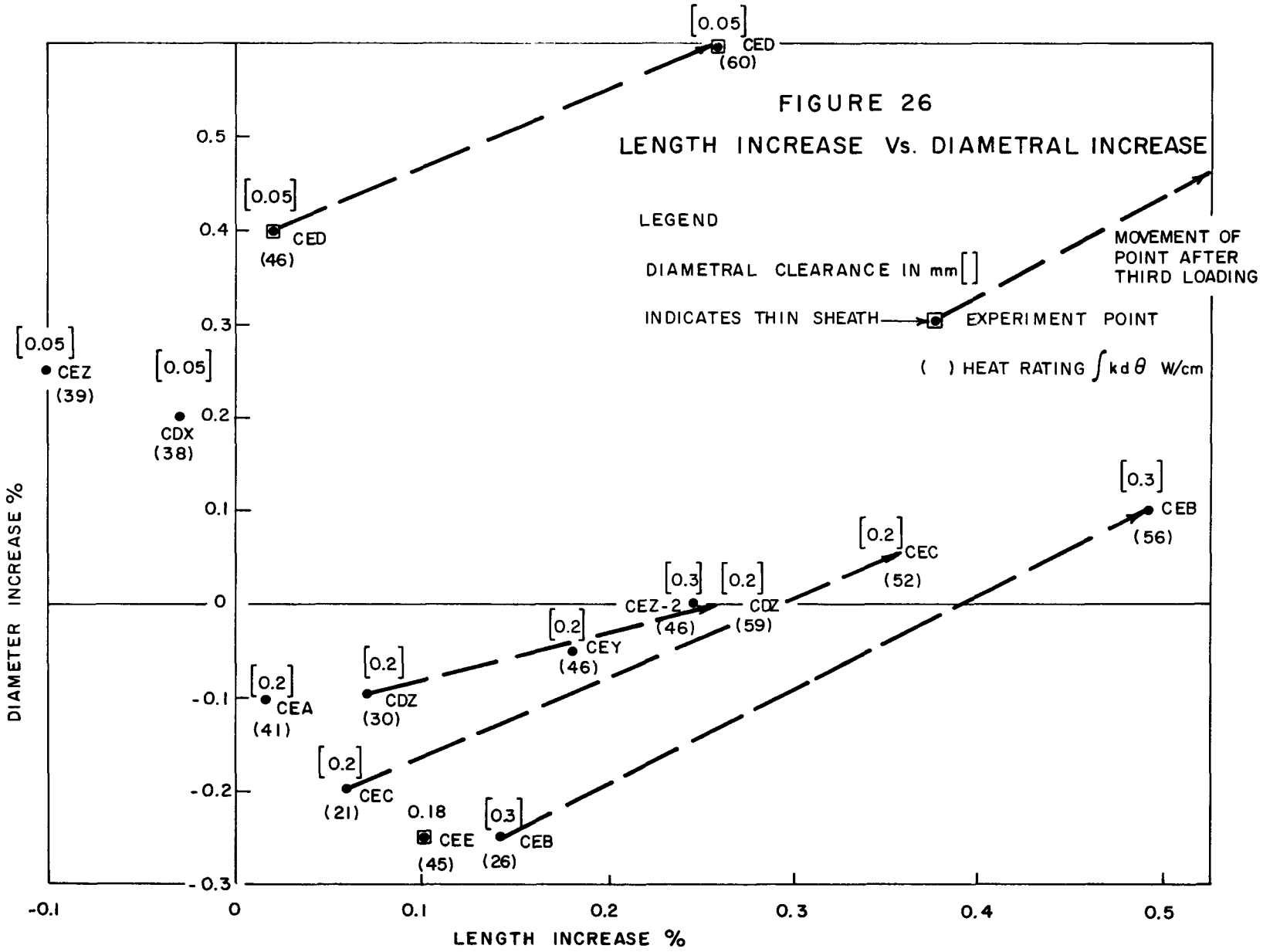
FIGURE 26
LENGTH INCREASE Vs. DIAMETRAL INCREASE
LEGEND
DIAMETRAL CLEARANCE IN mm[ ]
INDICATES THIN SHEATH
EXPERIMENT POINT
( ) HEAT RATING ∫kdθ W/cm
MOVEMENT OF POINT AFTER THIRD LOADING
[0.05] CED (60)
[0.05] CED (46)
[0.05] CEZ (39)
[0.05] CDX (38)
[0.3] CEB (56)
[0.2] CEC (52)
[0.3] [0.2] CEZ-2 (46) CDZ (59)
[0.2] CEY (46)
[0.2] CDZ (30)
[0.2] CEA (41)
[0.2] CEC (21)
0.18 CEE (45)
[0.3] CEB (26)
DIAMETER INCREASE %
LENGTH INCREASE %
0.5
0.4
0.3
0.2
0.1
0
-0.1
-0.2
-0.3
-0.1
0
0.1
0.2
0.3
0.4
0.5

FIGURE 27. CIRCUMFERENTIAL RIDGE HEIGHT Vs. $\int kd\theta$

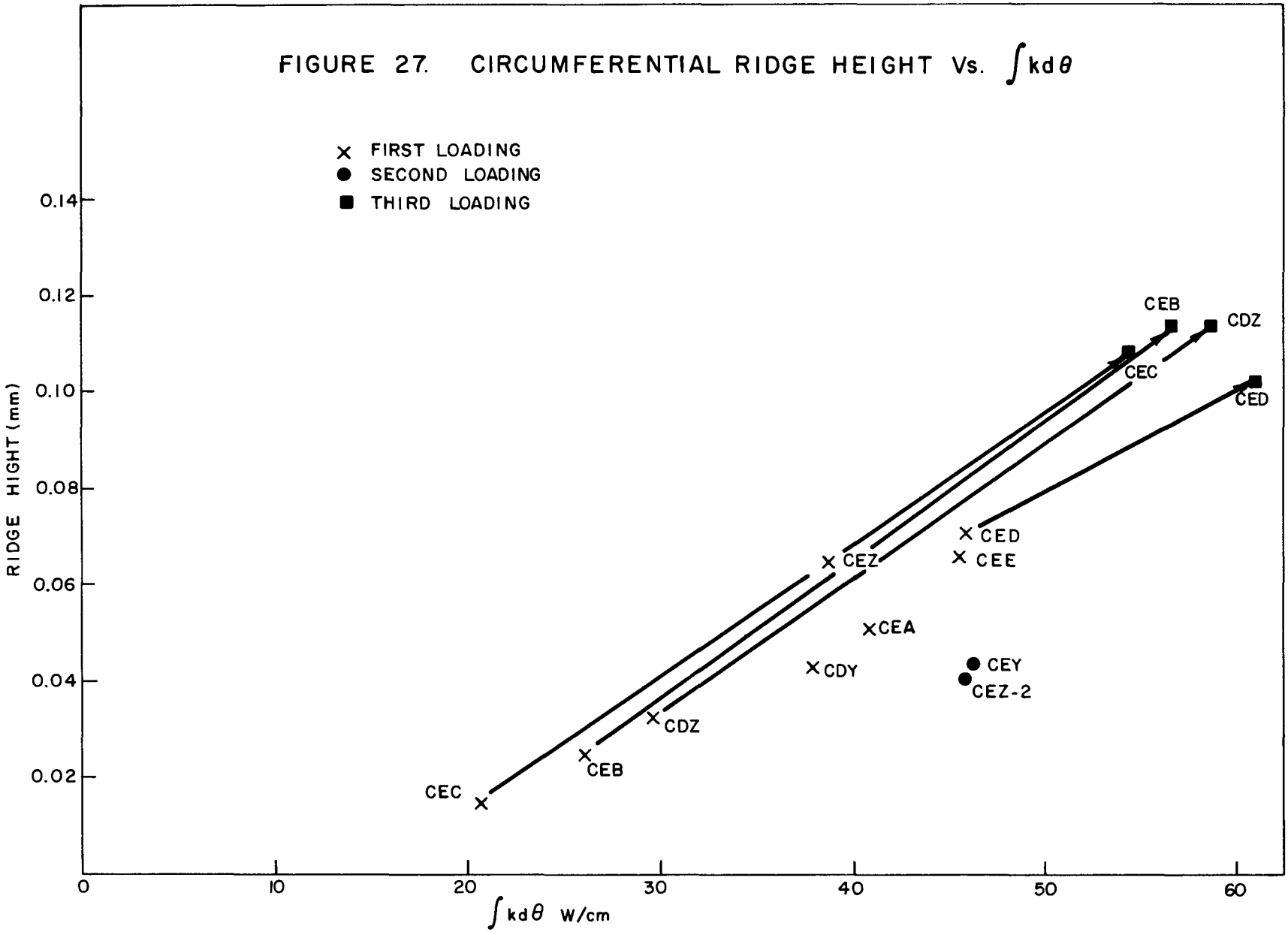

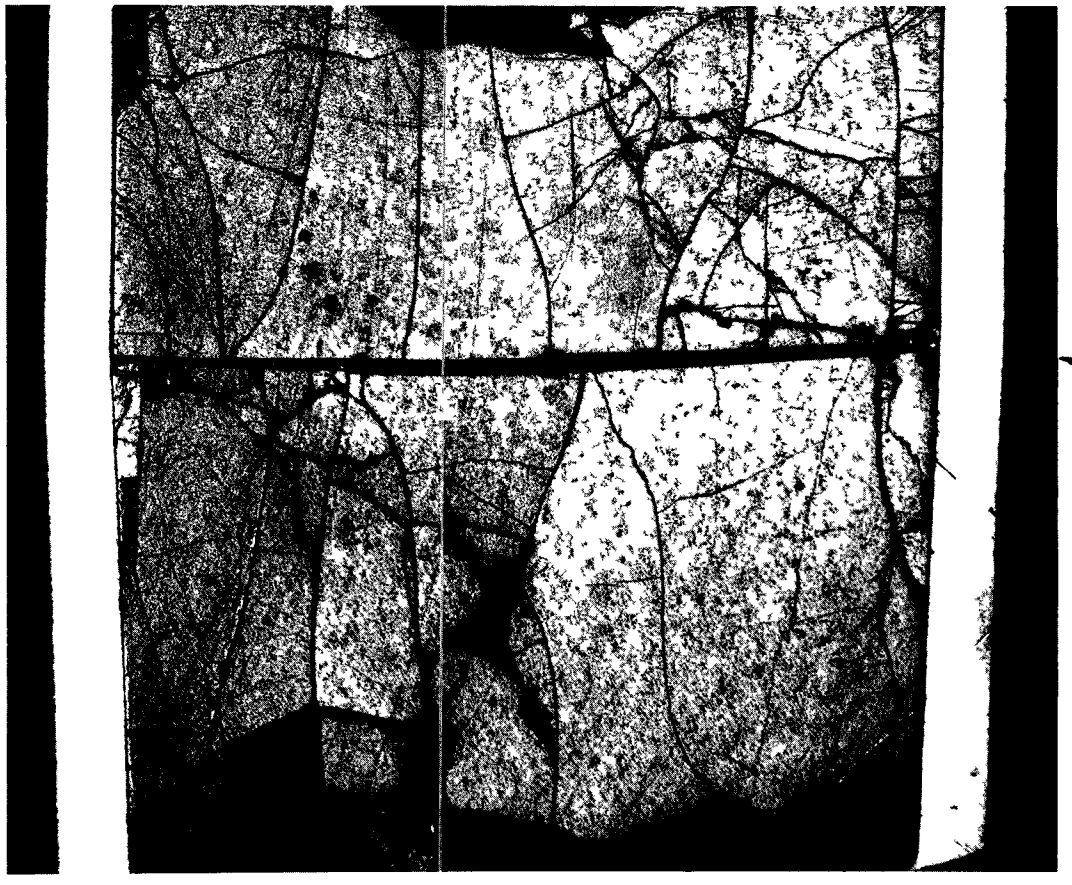

FIGURE 28: Pellet contour following sheath at circumferential ridge.

Reference Y-80-A-2 7.5X